Three-dimensional modeling of CPA to the multimillijoule level in tapered Yb-doped fibers for coherent combining systems

Alexey Andrianov,[1,2,*] **Elena Anashkina,**[1,2] **Arkady Kim,**[1,2] **Iosif Meyerov,**[2] **Sergey Lebedev,**[2] **Alexander Sergeev,**[1,2] **and Gerard Mourou**[2,3]

[1] *Institute of Applied Physics, Russian Academy of Sciences, 603950 Nizhny Novgorod, Russia*
[2] *Nizhny Novgorod State University, Nizhny Novgorod, Russia*
[3] *DGAR-IZEST, E'cole Polytechnique, Route de Saclay, F-91128 Palaiseau Cedex, France*
[*] *alex.v.andrianov@gmail.com*

Abstract: We developed a three-dimensional numerical model of Large-Mode-Area chirped pulse fiber amplifiers which includes nonlinear beam propagation in nonuniform multimode waveguides as well as gain spectrum dynamics in quasi-three-level active ions. We used our model in tapered Yb-doped fiber amplifiers and showed that single-mode propagation is maintained along the taper even in the presence of strong Kerr nonlinearity and saturated gain, allowing extraction of up to 3 mJ of output energy in 1 ns pulse. Energy scaling and its limitation as well as the influence of fiber taper bending and core irregularities on the amplifier performance were studied. We also investigated numerically the capabilities for compression and coherent combining of up to 36 perturbed amplifying channels and showed more than 70% combining efficiency, even with up to 11% of high-order modes in individual channels.

OCIS codes: (060.2320) Fiber optics amplifiers and oscillators; (060.7140) Ultrafast processes in fibers; (140.3298) Laser beam combining; (140.3615) Lasers, ytterbium; (140.7090) Ultrafast lasers.

References and links

1. G. Mourou, T. Tajima, M.N. Quinn, B. Brocklesby, and J. Limpert. "Are fiber-based lasers the future of accelerators?," Nuclear Instruments and Methods in Physics Research Section A: Accelerators, Spectrometers, Detectors and Associated Equipment **740**, 17–20 (2014).
2. L. Dong, X. Peng, and J. Li, "Leakage channel optical fibers with large effective area," J. Opt. Soc. Am. B **24**, 1689–1697 (2007).
3. J. Limpert, F. Stutzki, F. Jansen, H.-J. Otto, T. Eidam, C. Jauregui, and A. Tunnermann. "Yb-doped large-pitch fibres: effective single-mode operation based on higher-order mode delocalisation," Light: Science and Applications **1**, e8 (2012).
4. S. Fevrier, R. Jamier, J-M. Blondy, S.L. Semjonov, M.E. Likhachev, M.M. Bubnov, E.M. Dianov, V.F. Khopin, M.Y. Salganskii, and A.N. Guryanov, "Low-loss singlemode large mode area all-silica photonic bandgap fiber," Opt. Express **14**, 562–569 (2006).
5. H. Chen, T. Sosnowski, C. Liu, L. Chen, J. Birge, A. Galvanauskas, F. Kartner, and G. Chang, "Chirally-coupled-core Yb-fiber laser delivering 80-fs pulses with diffraction-limited beam quality warranted by a high-dispersion mirror based compressor," Opt. Express **18**, 24699–24705 (2010).

#222879 - $15.00 USD Received 16 Sep 2014; revised 19 Oct 2014; accepted 28 Oct 2014; published 6 Nov 2014

6. Filippov, V., Yu Chamorovskii, J. Kerttula, K. Golant, M. Pessa, and O. G. Okhotnikov. "Double clad tapered fiber for high power applications." Opt. Express **16**, 1929–1944 (2008).
7. J. Kerttula, V. Filippov, Y. Chamorovskii, V. Ustimchik, K. Golant, O.G. Okhotnikov. "Principles and performance of tapered fiber lasers: from uniform to flared geometry," Appl. Opt. **51**, 7025–7038 (2012).
8. A.V. Husakou, J. Herrmann, "Supercontinuum generation of higher-order solitons by fission in photonic crystal fibers," Phys. Rev. Lett. **87**, 203901–203901 (2001).
9. Ya. I. Khanin, *Fundamentals of Laser Dynamics*, (Cambridge Int Science Publishing, 2006)
10. J.W. Arkwright, P. Elango, G.R. Atkins, T. Whitbread, and M.J. Digonnet, "Experimental and theoretical analysis of the resonant nonlinearity in ytterbium-doped fiber," J. Lightwave Technol. **16**, 798 (1998).
11. M. Kuznetsov, O. Antipov, A. Fotiadi, and P. Megret, "Electronic and thermal refractive index changes in Ytterbium-doped fiber amplifiers," Opt. Express **21**, 22374–22388 (2013).
12. C. Schulze, A. Lorenz, D. Flamm, A. Hartung, S. Schroter, H. Bartelt, and M. Duparre, "Mode resolved bend loss in few-mode optical fibers," Opt. Express **21**, 3170–3181 (2013).
13. N.V. Didenko, A.V. Konyashchenko, A.P. Lutsenko, and S.Yu Tenyakov. "Contrast degradation in a chirped-pulse amplifier due to generation of prepulses by postpulses," Opt. Express **16**, 3178–3190 (2008).
14. D. Schimpf, E. Seise, J. Limpert, and A. Tunnermann, "The impact of spectral modulations on the contrast of pulses of nonlinearchirped-pulse amplification systems," Opt. Express **16**, 10664–10674 (2008).
15. J. Bourderionnet, C. Bellanger, J. Primot, and A. Brignon, "Collective coherent phase combining of 64 fibers," Opt. Express **19**, 17053–17058 (2011).
16. T. Eidam, C. Wirth, C. Jauregui, F. Stutzki, F. Jansen, H. Otto, O. Schmidt, T. Schreiber, J. Limpert, and A. Tünnermann, "Experimental observations of the threshold-like onset of mode instabilities in high power fiber amplifiers," Opt. Express **19**, 13218–13224 (2011).

1. Introduction

High peak power ultrashort pulse fiber amplifiers have attracted much attention in recent years. The interest is largely driven by growing applications of ultrashort pulse laser systems for material processing and new exciting applications of coherently combined high power fiber systems for high-field physics. Such a system utilizing thousands of chirped pulse fiber amplifiers which would finally deliver Joule level pulses at several kilohertz repetition rate compressed down to 200-300 fs duration is currently developed under the ICAN project (International Coherent Amplification Network) [1]. The overall system design implies that each individual channel delivers millijoule-level chirped pulses.

Large Mode Area (LMA) fibers are prominent candidates for high power and high energy chirped pulse amplifiers due to their reduced nonlinearity and lower damage threshold. However, achieving a large fundamental mode area usually implies existence of several higher order modes (HOM). Different techniques of higher order modes suppression were demonstrated, e.g., tight coiling, usage of a specially designed core structure (leakage channel fibers [2] and large-pitch fiber (LPF) [3]), bandgap fibers [4] and a chirally coupled core (CCC) fiber [5]), or very careful selective excitation of the fundamental mode by using passive mode field adapters and tapered active fibers. Tapered (conical) active fibers [6] have a strictly single mode core (approximately 7-10 μm in diameter) at the input, that gradually expands along the fiber up to several tens of microns supporting many modes at the output. Because of adiabatic mode transformation such fibers may be operated in an effectively single mode regime despite imperfect launching. Tapered active fibers may have also a double clad (DC) structure and thus support efficient multimode diode pumping. Since tapered fiber amplifiers provide sufficient flexibility combined with easy splicing to a single-mode seed source [7], they are prominent candidates for coherently combined multichannel setups where thousands of active fibers operate in a bundle. Comprehensive numerical simulations of individual amplifying channels, as well as of the whole coherently combined array would greatly help design the prospective high power laser system.

In this paper we developed a three-dimensional model for an LMA high energy broadband chirped pulse fiber amplifier accurately taking into account arbitrary refractive index profile, transverse active ion distribution, gain lineshape and gain depletion dynamics, as well as arbi-

#222879 - $15.00 USD Received 16 Sep 2014; revised 19 Oct 2014; accepted 28 Oct 2014; published 6 Nov 2014

trary material dispersion and Kerr nonlinearity. On the basis of the developed model, accurate modeling of high energy pulse amplification in LMA Yb-doped tapered fibers was done for the first time, to the best of our knowledge. We have shown that tapered amplifiers are capable of delivering up to 3 mJ of output energy in 1 ns pulses with a single mode transverse profile compressible down to 370 fs duration. Energy scaling and its limitations have been discussed. We have also investigated the amplified pulse compression and coherent combining of multiple channels taking into account spatiotemporal distortions.

2. The model

A comprehensive model of high energy chirped pulse amplification (CPA) in tapered active fibers must adequately describe pulse propagation taking into account variations of waveguiding properties along the length as well as nonlinear effects and gain dynamics.

The following issues have to be considered when developing the model:

1) Amplification of high power ultrashort pulses requires large stretching up to the nanosecond duration (larger stretching is not practical). Thus, the modeling grid has to be large enough to accommodate nanosecond pulses and provide subpicosecond resolution to track phase and intensity features vital for subsequent pulse compression and evaluation of compressed pulse quality.

2) Transverse distributions of electric field amplitude, refractive index and active ions which vary along the fiber need to be taken into account, so that mode structure and transverse variations of gain should be considered. The beam is strongly confined at the input of the tapered fiber but weakly guided at the output, therefore the model needs to handle both single-mode propagation and almost free-space diffraction as well. Variation of waveguiding properties along the distance makes it difficult to apply the modal decomposition approach.

3) Gain line shape and its time and spatial variations owning to population dynamics may have a strong impact on output pulse parameters due to relatively large signal bandwidth and pulse energy.

4) Gain saturation and population inversion depletion during amplification of high energy pulses are significant for evaluation of output pulse energy.

5) Kerr nonlinearity may have a strong impact on spatiotemporal pulse dynamics and resulting pulse quality.

To address the above problems we developed a time and frequency resolved beam propagation model for multimode waveguides of arbitrary shape. In the following we present a detailed description of our model.

Assume that the linear refractive index of the fiber is given in the form

$$n(x,y,\omega) = n_0(\omega) + \Delta n(x,y,z,\omega),$$

where x,y are Cartesian coordinates in the fiber cross section, z is the coordinate along the fiber and ω is angular frequency. The refractive index of the fiber inner cladding made of silica is given by n_0, and an additional refractive index of the fiber core is described by Δn. When considering the signal propagation we will not take into account the second cladding of the DC fiber, which is only needed to confine the pump light. Note that pump light propagation may be modeled separately and used to calculate initial population inversion.

We assume that linearly polarized electric field E has the form

$$E(x,y,z,t') = \mathrm{Re}(A(x,y,z,t')\exp(ik_0 z - i\omega_0 t')), \tag{1}$$

where $A(x,y,z,t')$ is the complex field amplitude, t' is time, ω_0 is carrier optical frequency, and $k_0 = \omega_0 n_0(\omega_0)$. We also introduce Fourier transforms of the fields in time and transverse

#222879 - $15.00 USD Received 16 Sep 2014; revised 19 Oct 2014; accepted 28 Oct 2014; published 6 Nov 2014

coordinate domains:

$$A_\omega(x,y,z,\omega) = \hat{F_\omega}[A(x,y,z,t)], \tag{2}$$

where

$$\hat{F}_\omega[A] = \frac{1}{\sqrt{2\pi}} \int_{-\infty}^{+\infty} A(x,y,z,t)\exp(i\omega t)dt, \tag{3}$$

$$A_k(k_x,k_y,z,t) = \hat{F}_k[A(x,y,z,t)], \tag{4}$$

where

$$\hat{F}_k[A] = \frac{1}{2\pi} \int_{-\infty}^{+\infty} A(x,y,z,t)\exp(-ik_x x - ik_y y)dxdy \tag{5}$$

and combined spatiotemporal transform $\hat{F}_{\omega k} = \hat{F}_\omega \hat{F}_k$.

We used the unidirectional wave propagation equation [8] with additional gain term to describe the evolution of broadband signal in irregular waveguide:

$$\frac{\partial A_{\omega k}(k_x,k_y,z,\widetilde{\omega})}{\partial z} = i(\sqrt{\omega^2 n_0(\omega)^2/c^2 - k_x^2 - k_y^2} - k_0 - k_1\widetilde{\omega})A_{\omega k} +$$
$$+ i\hat{F}_k[\omega A_\omega(x,y,z,\widetilde{\omega})\Delta n(x,y,z,\omega)/c] + i\hat{F}_{\omega k}[\omega_0 n_2 A(x,y,z,t)|A(x,y,z,t)|^2/c] + \hat{F}_k[G(A)] \tag{6}$$

Here, the first term in the right-hand side is responsible for the propagation in an unbounded medium with refractive index n_0, where the fast phase evolution and pulse propagation with group velocity are compensated by k_0 and $k_1 = \partial_\omega(\omega n_0(\omega)/c)|_{\omega=\omega_0}$, respectively, and we have introduced relative frequency $\widetilde{\omega} = \omega - \omega_0$ and retarded time $t = t' - k_1 z$. The second term accounts for an additional refractive index of the fiber core, the third term represents Kerr nonlinearity, where n_2 is the nonlinear refractive index, and the last term represents gain and is discussed later.

Gain dynamics may have a strong influence on high energy pulse amplification. Gain depletion becomes significant for the pulse energies comparable with the saturation energy, which is roughly 0.5 mJ for an Yb doped fiber with the mode field diameter (MFD) of 50 μm. It is also well known that spectral gain shape for a quasi-three-level system (Yb-doped silica glass is an example of such systems) depends on the excitation level or fraction of atoms in the population inversion, which in turn changes in time while energy is transferred to the amplified pulse. We propose a relatively simple and computationally efficient model of gain based on a phenomenological extension of semi-classical Maxwell-Bloch equations. The following assumptions are essential for deriving the model. First, we assume the system to be an effectively two-level one (two Stark-split manifolds) with populations at ground and laser levels $N\rho_1$ and $N\rho_2$, respectively, where N is total active ion density, and ρ_1, ρ_2 are relative populations ($\rho_1 + \rho_2 = 1$). Second, we assume that values of ρ_1 and ρ_2 are known before arrival of the pulse ($t = -\infty$ in the modeling) and do not depend on the previous pulses in train, which is fairly true for amplifiers with low repetition rate, where the pump is synchronized with the pulse train. Third, we neglect pump action and spontaneous emission processes on the time scale of the amplified pulse. The gain term in Eq.(6) can be represented in the form $G = i2\pi\omega_0 P/(cn_0(\omega_0))$, where P is the polarization of active ions.

Let us recall the equation for polarization P in a two-level homogeneously broadened system [9]:

$$\frac{\partial P(t)}{\partial t} + \left[\frac{1}{T_2} - i(\omega_0 - \omega_{21})\right] P(t) = -\frac{id^2 N}{\hbar} A(t)\Delta\rho(t) \tag{7}$$

#222879 - $15.00 USD Received 16 Sep 2014; revised 19 Oct 2014; accepted 28 Oct 2014; published 6 Nov 2014

Here T_2 is dephasing time, ω_{21} is the central frequency of the laser transition, $\hbar$ is Planck's constant, d is transition dipole moment and $\Delta\rho = \rho_2 - \rho_1$ is the fraction of the inverted atoms. In the frequency domain, Eq.(7) is readily solved for P:

$$P_\omega(\widetilde{\omega}) = -iN(x,y,z)L(\widetilde{\omega})\hat{F_\omega}[A(t)\Delta\rho(t)], \tag{8}$$

where the function $L(\widetilde{\omega}) = d^2\hbar/(1/T_2 - i(\widetilde{\omega} + \omega_0 - \omega_{21}))$ describes homogeneous broadening. Being inserted into Eq.(6) this equation gives

$$\frac{\partial A_{\omega k}(x,y,z,\widetilde{\omega})}{\partial z} = \frac{\sigma_L + i\beta}{2} N(x,y,z)\hat{F_\omega}[A(t)\Delta N(t)], \tag{9}$$

where we have omitted all propagation and Kerr terms for a while and returned to the coordinate representation. Here $\sigma_L = 2d^2\pi\omega_0/(\hbar c n_0[1/T_2^2 + (\widetilde{\omega} + \omega_0 - \omega_{21})^2])$ defines homogeneous Lorentzian line shape, and β (imaginary part) describes refractive index variation of active ions. Now we step further and replace the homogeneous Lorentzian cross section σ_L by effective emission and absorption cross sections (σ_a and σ_e, respectively) combined with population values at the corresponding laser level, which gives

$$\frac{\partial A_\omega(x,y,z,\widetilde{\omega})}{\partial z} = G = \frac{N(x,y,z)}{2}\left((\sigma_e(\omega) + i\beta_1)\hat{F_\omega}[A(t)\rho_2(t)] - (\sigma_a(\omega) + i\beta_2)\hat{F_\omega}[A(t)\rho_1(t)]\right). \tag{10}$$

The imaginary parts β_1, β_2 may have contributions from laser transition itself (may be evaluated by using the Kramers-Kronig relations) [10] and also from other transitions (even with resonant frequencies lying quite far from ω_0) whose polarizability depends on excitation at lasing levels [11]. Unlike σ_a and σ_e which were accurately measured in active fibers with different glass compositions, quantities β_1 and β_2 are only known by the order of magnitude.

For stationary ρ_1, ρ_2, Eq.(10) describes the dependence of combined gain and reabsorption line shape on frequency and the fraction of atoms at the ground and laser levels for quasi-three-level systems.

The population dynamics is easily accessed by utilizing the energy conservation law. Energy increase of a small portion of the pulse with dimensions dx, dy and time duration dt propagating from z to $z + dz$ is proportional to the number of atoms that jumped from the upper to the lower state in the volume $dxdydz$ during time dt.

Rewriting the rate of energy increase due to gain using Eq.(6) yields the following equation

$$\frac{N(x,y,z)\hbar\omega_0}{2\pi n_0 c}\frac{\partial\rho_2(x,y,z,t)}{\partial t} = -\left(\frac{\partial|A(x,y,z,t)|^2}{\partial z}\right)_{Due\ to\ gain}. \tag{11}$$

Note that the above equation accounts for both emission and absorption processes, therefore it can be used to simulate in-band pumping of quasi-three-level systems. Equation (6), where the gain term is defined according to Eq.(10), and equation (11) form a self-consistent system for modeling spatiotemporal pulse dynamics in the fiber amplifier.

3. Numerical algorithm

Numerical implementation of the developed model is based on the split-step Fourier method in which the propagation term is easily handled in the transverse wavenumber-frequency domain, waveguiding refractive index of the core and gain term are treated in the transverse coordinate-frequency domain, and Kerr nonlinearity in the coordinate-time domain. In parallel, population distribution over transverse coordinates and time is computed at each propagation step. The efficient numerical code was developed for multi core CPU systems with shared memory utilizing the advantages of parallel computation. Large enough grids up to 128x128x32768 points

#222879 - $15.00 USD Received 16 Sep 2014; revised 19 Oct 2014; accepted 28 Oct 2014; published 6 Nov 2014

(x,y,t) were used to capture features of the amplification process. Numerical simulations were performed on the "Lobachevsky" supercomputer at the University of Nizhny Novgorod. We used up to 45 computational nodes with the following configuration: 2x Intel Xeon E5-2660 CPU (8 cores, 2.2 GHz), 64 GB RAM, OS Windows HPC Server 2008. Computational cores of a node were utilized using OpenMP. Performance-critical loops were vectorized by the Intel C++ Compiler from Intel Parallel Studio XE 2013 using Advanced Vector Extensions (AVX). FFTW library was used for computing the discrete Fourier transform. Modeling of 0.5 meter fiber with longitudinal resolution of 10 μm takes approximately 60 hours using one computational node.

4. Simulation results

First, we investigated the amplification of broadband highly chirped pulses with high peak power in short pieces of a tapered active fiber in order to learn the influence of multimode propagation in the presence of strong Kerr nonlinearity and high gain. We studied the amplification of a 0.5 ns Gaussian pulse with a large quadratic phase corresponding to 250 fs transform-limited duration. Realistic parameters of gain corresponding to Yb doping of about 1%, maximum small-signal absorption of 600 dB/m (for unpumped fiber at 976 nm) and saturation energy of 0.5 mJ for 50 μm MFD were included. At this point, we neglected the influence of refractive index variations due to population dynamics, i.e. assumed $\beta_1 = \beta_2 = 0$. Initial inversion was set to 0.5 at 976 nm transition along the whole fiber, which is the maximum value achievable with 976 nm pump. The distribution of pump intensity along and across the fiber may be non-uniform. Nevertheless, for high enough input pump power, high pump light intensity is maintained along the fiber, therefore the transition at 976 nm is saturated, and the initial inversion approaches the same saturated value along the whole fiber. As we are mainly interested in evaluation of maximum achievable pulse energy limited by nonlinearities we reasonably assume that high enough pump power is provided.

The amplification of 5 μJ pulses centered at 1030 nm in 0.5 meters of active fiber taper is shown in Fig. 1. The fiber has a slightly smoothed step-index profile with $\Delta n = 1.45 \times 10^{-3}$ (NA=0.065) (see Fig. 1(b)). Its diameter linearly increases from 10 μm, supporting only the fundamental mode at the input to 60 μm at the output supporting 21 modes at 1030 nm. In real fibers the refractive index profile may deviate from step-index and strongly depends on the preform fabrication and fiber drawing process, although very close to step-index profiles are achievable experimentally. Our numerical code allows modeling a fiber with arbitrary refractive index profile which in practice may be taken from the experimental data. For modeling the main features of multimode propagation in the presence of strong nonlinearities and fiber perturbations we first use a smoothed step-index profile as a simple yet reasonable approximation. It is seen from Fig. 1 that the pulse, indeed, propagates in a single-mode regime while its energy increases about 157 times up to 0.8 mJ. Its peak intensity grows slower because of increasing MFD and reaches 230 GW/cm^2 at the output. The integration of the output field profile with eigenmodes of the 60 μm fiber shows that more than 98% of output energy is contained in the fundamental mode.

The pulse experiences strong self-phase modulation (SPM) manifested in the increasing difference of the pulse chirp from the linear one shown in Fig. 1(f). The additional phase shift acquired by the pulse due to SPM is large (12 π at maximum with respect to the pulse wings), which results in the need for careful high order phase compensation at compressor stage. However smooth time, spectral and spatial distributions (see Figs. 1 (d) and 1 (e)) are maintained along the whole taper.

From above we can conclude that neither strong Kerr nonlinearity nor saturated gain lead to excitation of high-order modes in an ideal tapered amplifier.

#222879 - $15.00 USD Received 16 Sep 2014; revised 19 Oct 2014; accepted 28 Oct 2014; published 6 Nov 2014

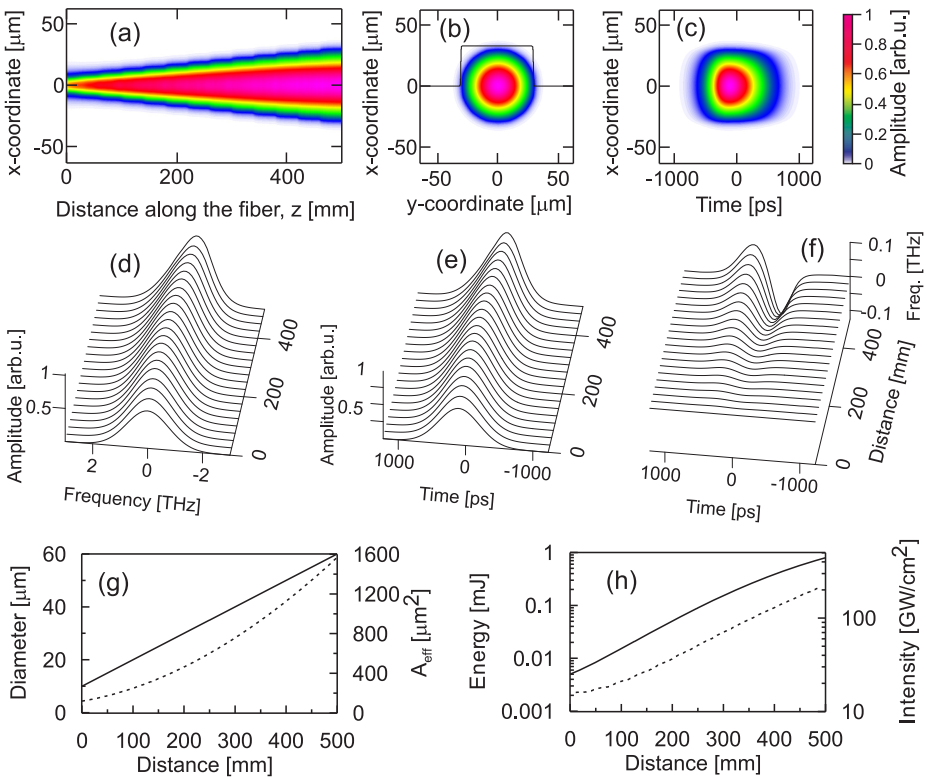

Fig. 1. Amplification of 0.5 ns pulses in 0.5 meter long tapered fiber: (a) distribution of field amplitude at $y = 0$, $t = 0$ along the fiber, (b) transverse output field distribution at the time corresponding to absolute pulse maximum, (c) distribution of output field amplitude at $y = 0$ as a function of x and t, (d) evolution of pulse temporal profile at the core center, (e) evolution of spectral amplitude at the core center, (f) evolution of nonlinear frequency modulation at the core center, (g) fiber diameter (solid line) and effective area of fundamental mode A_{eff} (dashed line), (h) total pulse energy (solid line) and peak intensity (dashed line). Note that color maps represent amplitude (square root of intensity) distributions.

To study the influence of different perturbations, which may lead to multimode propagation and transverse profile distortion, we modeled the effects of bending and irregularities of a tapered fiber. The impact of macrobending was included in the model as additional refractive index variation $\Delta n_b = n_0 x/R_{eff}$, where R_{eff} is effective curvature radius in the (x,z) plane [12]. Figures 2(a)–2(c) illustrates the effect of bending with the radius of curvature linearly increasing from 10 cm at the input to 60 cm at the output (the output end of the taper is much stiffer and harder to bend). Noticeable distortion of the fundamental mode and reduction of its area are evident, especially closer the output end. However, no signs of distinguishable HOM excitation are seen on the entire fiber length. The output signal profile shows no intermodal interference both in spatial and temporal representations. Next, microbending and irregularities of the fiber core were included in the model. To do so we modeled a regular shift of the fiber core with amplitude of 4 μm and period increasing from 5 cm at the input end to 12 cm at the output (see Figs. 2(d)–2(f)). Then, random jitter of the centerline of the fiber core with the RMS amplitude of 0.3 μm and peak-to-peak amplitude of 1 μm was added. Figures 2(g)–2(i) shows noticeable excitation of many HOMs along the fiber. The output signal profiles show degradation of spa-

#222879 - $15.00 USD Received 16 Sep 2014; revised 19 Oct 2014; accepted 28 Oct 2014; published 6 Nov 2014

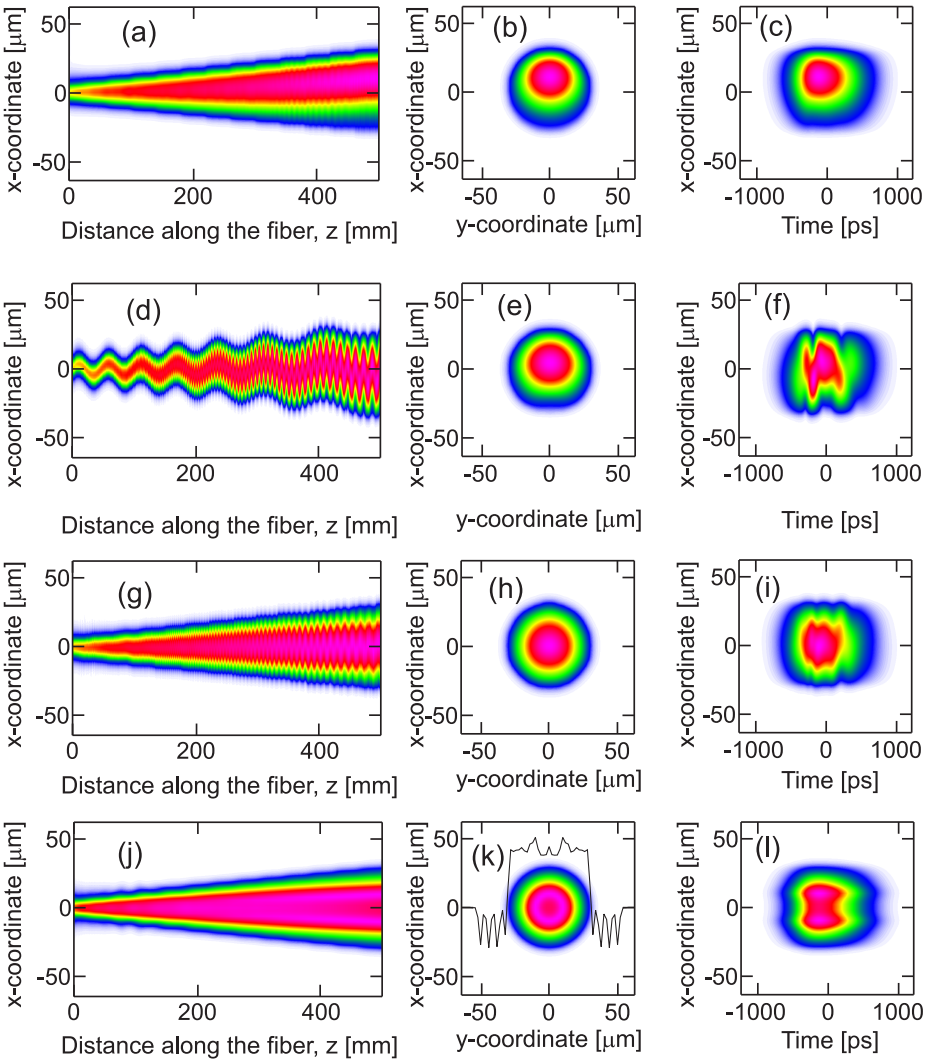

Fig. 2. The influence of different perturbations on the mode structure and spatiotemporal distortions during amplification of 0.5 ns pulse in tapered fiber: (a) distribution of field amplitude at $y = 0$ along the fiber, (b) transverse output field distribution at the time corresponding to the absolute pulse maximum, (c) distribution of output field amplitude at $y = 0$ as a function of x and t; (d,e,f) - the same as (a,b,c) but for the fiber bent with the radius increasing from 10 cm to 60 cm; (g,h,i) - the same as (a,b,c), but for the fiber with regular core shift from the centerline with amplitude of 4 μm; (g,h,i) - the same as (a,b,c) but for the fiber with random core shift from the centerline (peak-to peak amplitude of variations is 1 μm); (i,k,l) - the same as (a,b,c) but for the fiber with complicated refractive index profile fitted to the one measured in the preform.

tial and temporal beam quality originating from the interference of many modes that acquired different phases and time delays along the fiber length. However, the overall picture of nonlinear Kerr interaction has not significantly altered compared to the pure single-mode case. We verified that the nonlinear chirp acquired by the pulse is almost the same as in an unperturbed amplifier.

#222879 - $15.00 USD Received 16 Sep 2014; revised 19 Oct 2014; accepted 28 Oct 2014; published 6 Nov 2014

Then, we modeled imperfectness of the transverse distributions of active ions and dopants that form the waveguiding core. The refractive index profile shown in Fig. 2(k) was constructed as a combination of trigonometric and hyperbolic functions and resembles the measured profile of one of the fiber preforms. Active ion distribution was also fitted by a similar function. Numerical modeling shows noticeable distortion of the fundamental mode and its increased sensitivity to bending because of the refractive index dip in the middle of the core. Nevertheless, no excitation of HOMs or significant distortions of the spatiotemporal structure of the pulse were observed.

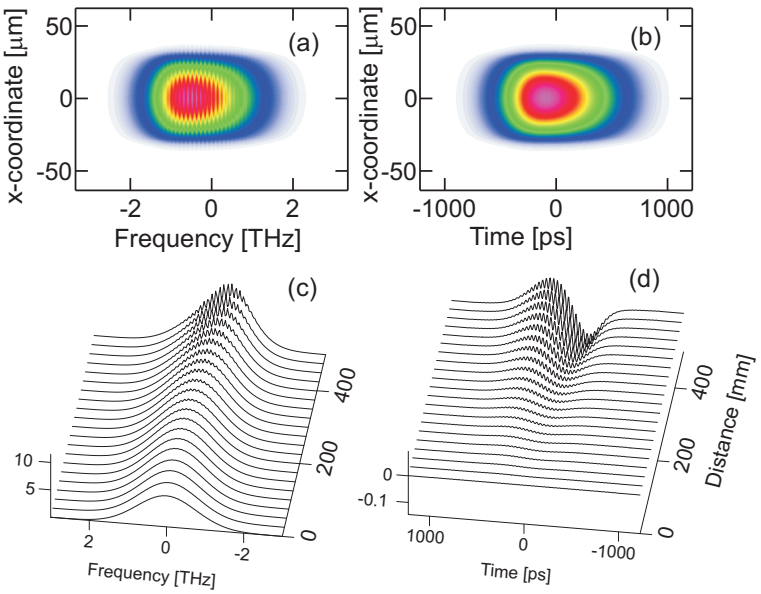

Fig. 3. Distortions of the spectrum and the chirp of the pulse with postpulse (50 dB lower intensity at the input) due to nonlinear phase resulting from SPM: (a) Distribution of output field amplitude at $y = 0$ as a function of x and t , (b) output spectrum at $y = 0$, (c) spectrum evolution at the core center, (d) frequency modulation evolution at the core center.

More important, we confirmed that even shallow small-scale modulation of input intensity distribution may result in severe distortions of spectral intensity, spectral and temporal phase profiles (see Fig. 3). One potential source of the small scale amplitude modulation on the stretched pulse is interference between the main pulse and its delayed replica which may arise from parasitic reflections or polarization mode beating in the preceding PM fibers. Then, small intensity modulation is converted by Kerr nonlinearity into phase modulation in the time domain, which also leads to modulation of the spectrum and spectral phase. The effect of small scale modulation resulting in subsequent temporal contrast degradation and generation of multiple pre- and postpulses after the compression was investigated previously theoretically and experimentally for a bulk chirped pulse amplifier [13] and fiber amplifiers [14]. Nevertheless, 3D modeling shows (see Fig. 3) that the pulse distortions occur purely in temporal and spectral domains and do not alter the spatial field distribution. Hence, a much simpler one-dimensional model may be used to study this phenomenon and results of the previous research [14] provide good estimate for the trade off between the amount of SPM and the pulse quality.

Next, energy scaling to the multi-millijoule level keeping peak intensity at a admissible level was studied. By using an extremely large grid (32768 points) in time domain we used our model for amplification of 1 nanosecond Gaussian highly chirped pulses with 250 fs compressed du-

#222879 - $15.00 USD Received 16 Sep 2014; revised 19 Oct 2014; accepted 28 Oct 2014; published 6 Nov 2014

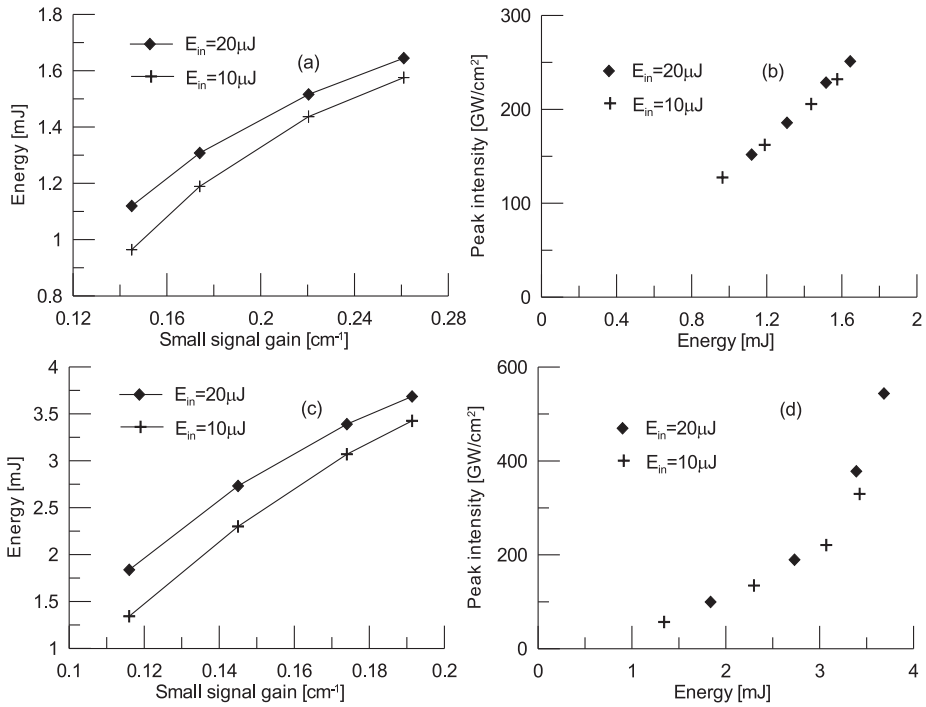

Fig. 4. Energy scaling of 1 ns pulses: (a) output energy from 10-60 μm taper versus small signal gain at 1030 nm for input pulse energy 10 μJ (crosses) and 20 μJ (rhombs), (b) maximum peak intensity at the output of 10-60 μm taper as a function of output energy, (c) and (d) - the same as in (a) and (b) but for 10-110μm taper.

ration. We performed several numerical experiments with two values of input pulse energy (10 μJ and 20 μJ) and different values of small-signal gain at 1030 nm. Different values of small signal gain correspond to different Yb doping or, less precisely, to different values of initial inversion at the same doping (variation of initial inversion also affects gain line shape). Figure 4 shows the output energy versus the small-signal gain obtained in the modeling. By increasing the seed pulse energy and small-signal gain we obtained almost double increase in the output energy from 0.96 mJ up to 1.66 mJ. However, the maximum nonlinear phase shift of 12π would make it difficult to compress the pulse and maintain its quality in the presence of even small modulation. It is seen from Fig. 4 that amplification occurs in the saturation regime, thus for ideal 0.5-meter taper and ideal 1 ns input pulse, maximum extractable energy is limited mainly by saturation effects. Depending on the input pulse quality, energy scaling may be also limited by the small scale nonlinear phase and spectral distortions.

In an attempt to further increase mode field diameter and therefore active volume we modeled the fiber tapered from 10 to 110 μm (see Fig. 5). Two cases with the input energy of 10 μJ and 20 μJ were studied. Up to 3.0 mJ and 3.4 mJ at the output were obtained for those cases, respectively. Modeling shows that a very large core is not robust against the mode structure distortion due to Kerr refractive index changes. Pronounced mode field size reduction and small excitation of several radial modes were observed, especially for the 3.4 mJ output. Noticeable fast increase in peak intensity up to 380 GW/cm^2 closer to the output end clearly indicates the onset of self-focusing. Although, the spatiotemporal distribution was not strongly affected and the total nonlinear phase shift was about 6π and 8π for the first and second cases, respectively.

#222879 - $15.00 USD Received 16 Sep 2014; revised 19 Oct 2014; accepted 28 Oct 2014; published 6 Nov 2014

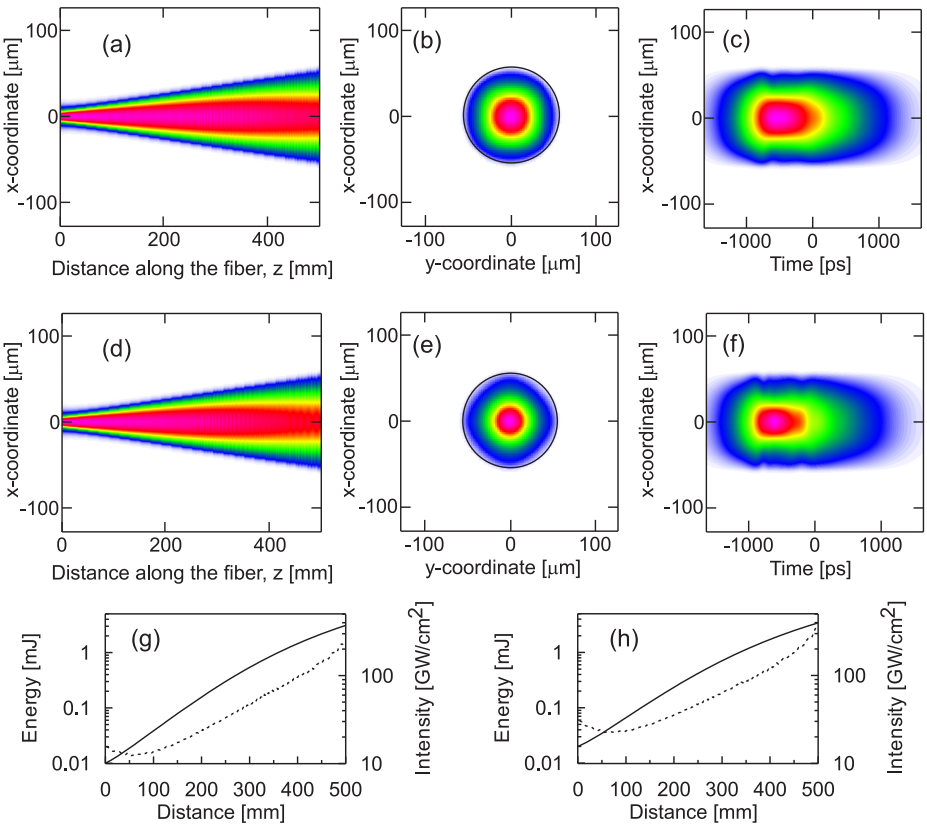

Fig. 5. Amplification of 10μJ 1 ns pulses in 10-110 μm taper: (a) distribution of field amplitude at $y = 0$,$t = 0$ along the fiber, (b) transverse output field distribution at the time corresponding to the absolute pulse maximum, (c) distribution of output field amplitude at $y = 0$ as a function of x and t, (g) the pulse energy (solid line) and peak intensity (dashed line). The same for 20μJ input pulse (d,e,f,h).

Further increase in either input energy or gain lead to self-focusing at the output. Thus, in tapers with very large output diameter and weakly guiding core, self-focusing set an ultimate limit for maximum output energy.

We believe that further scaling of the pulse energy to 5-10 mJ is possible by stretching the pulse to practically suitable duration of several nanoseconds.

In order to verify CPA applicability to tapered amplifiers we modeled pulse compression at the output. We assume that linear and nonlinear chirp may be perfectly compensated at the core center so we subtracted the same spectral phase from all the points in the transverse plane. Although it is not an easy task in real experiments, in principle, fine tuning of spectral phase in a compressor can be done by using spatial light modulators (SLM). The resulting pulse shapes for different conditions are shown in Fig. 6. As a reference we used 1.5 mJ output from an ideal taper, which can be compressed down to 370 fs (blue curve in Fig. 6(a)). The excitation of HOMs in a perturbed amplifier (regular core shift as in Fig. 2(c)) results in appearance of pulse wings and contrast degradation. Distortions are also seen in the spatiotemporal structure, especially at some distance from the beam center, where the influence of asymmetric modes is higher. Interestingly, even in the presence of noticeable HOM content, the main pulse can be compressed to almost the same duration as in the unperturbed case. Figure 6(b) illustrates

#222879 - $15.00 USD Received 16 Sep 2014; revised 19 Oct 2014; accepted 28 Oct 2014; published 6 Nov 2014

compression of 3 mJ pulses from a 10-110 μm taper. The spatiotemporal distribution shows slightly higher distortions at the beam center, nevertheless, the pulse can be compressed to 380 fs.

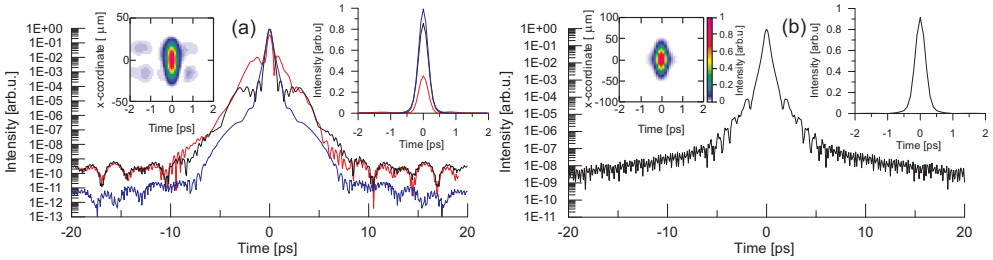

Fig. 6. Compression of pulses amplified in 10-60 μm tapers: (a) temporal profile of ideally compressed pulse after unperturbed amplifier (blue curve), compressed pulse after irregular taper at the core center (black curve) and in 10 μm off-center position (red curve). Compression of the pulse amplified in 10-110 μm taper (b). Insets show spatiotemporal intensity distributions and compressed pulse profiles on linear scale.

5. Coherent combining

We also investigated coherent combining of several beams delivered by tapered fiber amplifiers. Since 3D modeling enables studying beam combining with transverse field distribution taken into account, we mainly focused on the influence of HOM generation due to fiber irregularities in the presence of strong Kerr nonlinearity and gain. Other effects, including dephasing and time-of-flight jitter due to input power or gain variations may be investigated with reasonable accuracy in a one-dimensional model and are outside the scope of our study. We simulated numerically up to 36 channels with equal input power and gain, but with different random fiber irregularities (as presented in Fig. 2) leading to HOM excitation. Irregularities may result from mechanical vibrations and nonstationary thermal effects leading to random variations of refractive index of the fiber. Total phase shift in each channel may be compensated by phase modulators with properly arranged feedback, but the excitation of HOMs giving rise to differential phase and time delays across the transverse profile cannot be compensated by any simple means.

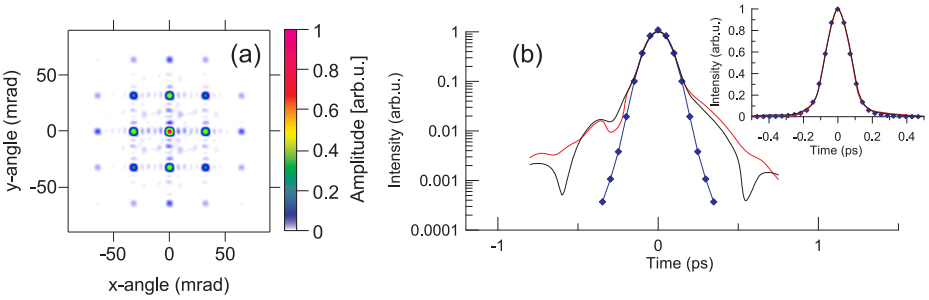

Fig. 7. Far field pattern of 36 combined channels: (a) temporal intensity distributions of combined and compressed pulses, (b) combined and compressed pulse (red curve), compressed pulse in one individual perturbed channel (black curve), compressed pulse from unperturbed amplifier (blue rhombs). Inset shows compressed pulse profiles on linear scale.

#222879 - $15.00 USD Received 16 Sep 2014; revised 19 Oct 2014; accepted 28 Oct 2014; published 6 Nov 2014

For each channel collimation by a thin lens with hard square aperture was modeled. Then the beams were arranged in a two-dimensional grid, and a far field zone was calculated by using the Fourier transform. Arrangement of the numerical experiment closely resembles the one used in the recent experimental study of summation of 64 CW fiber channels collimated with a lens array and combined in a far field [15]. We also modeled compression of combined chirped pulses back to femtosecond duration. We assume that for the pulse amplified in an unperturbed fiber it is possible to perfectly compensate its chirp, including the nonlinear one originating from SPM and dispersion. In our modeling, spectral phase of the unperturbed pulse (taken at the pulse center in the transverse coordinates) was recorded and then subtracted from all channels. Far-field distribution for 36 channels arranged in a square grid is shown in Fig. 7. Well defined central maximum and several distinct side lobes are clearly seen along with a very weak irregular background originating from imperfect field distributions with some higher order mode content of individual channels. Time profile of the compressed pulse taken at the center of the main maximum in the far-field pattern is also shown in Fig. 7. One can see that although the pulse quality is not perfect, no further degradation occurs after combining.

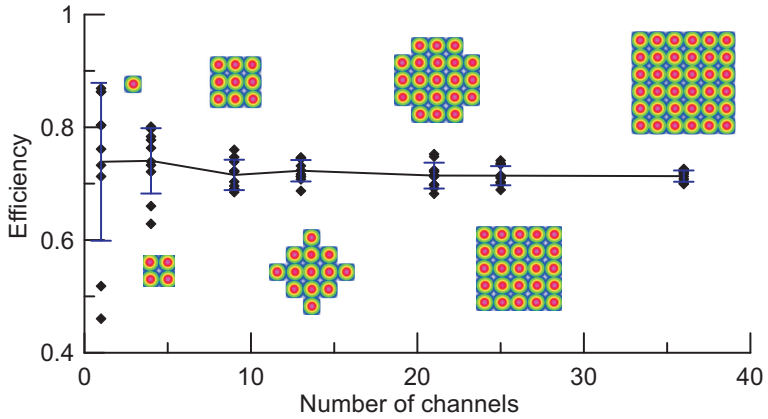

Fig. 8. Combining efficiency as a function of the number of combined channels. Insets show beam arrangement patterns.

Next, we studied the efficiency of compression and combining of perturbed tapered fiber amplifiers. For characterization of the process we used the ratio of peak intensities obtained after compression and combining of perturbed pulses and the same number of ideal pulses. Figure 8 shows the efficiency for a different number of combined channels. The corresponding beam arrangement patterns are shown in the insets. For each number of channels, we made several numerical experiments with different implementations of random perturbations. It is seen that, for an increasing number of channels, average efficiency stabilizes at some level and its dispersion gradually decreases. For given perturbations, the combining efficiency is as high as 72% while excitation of HOMs in the amplifier reaches 11% (i.e. only about 89% of the pulse energy in each channel propagates at the fundamental mode).

6. Discussion

The presented modeling shows that short active tapered fibers are capable of amplifying strongly chirped pulses up to several mJ with single mode quality even under strong influence of Kerr nonlinearity and gain saturation. Moderate perturbations of refractive index profile results in predictable distortions of the output pulse and do not severely affect the amplification process. In principle, in a perfectly tapered amplifier, energy scaling with reasonably small ex-

#222879 - $15.00 USD Received 16 Sep 2014; revised 19 Oct 2014; accepted 28 Oct 2014; published 6 Nov 2014

citation of HOMs is possible up to ultimate self-focusing limit. However, further investigations and model improvements are desirable.

First, pump light propagation and initial inversion distributions across and along the fiber are of great interest for evaluation of achievable small-signal gain, energy conversion efficiency and heat dissipation. We believe that high value of initial inversion needed for obtaining high gain in a short taper may be achieved by using high brightness multimode diodes for backward pumping of double clad taper with a low clad-to-core ratio. Additionally, single mode diodes and conventional WDMs may be used to pump the taper from the thin end. Modeling of pump light propagation may be performed on the basis of our model with simple modification taking into account the first and second cladding.

Then, the influence of stimulated Raman scattering (SRS) leading to energy transfer to longer wavelengths should be investigated. Estimations show that for 3.4 mJ pulse in 10-110 μm taper, maximum Raman gain at the pulse center integrated over the fiber length and cross-section is about 60 dB, and it drops to about 40 dB for 3.0 mJ pulses. This estimation suggests that SRS limit is one of the main concerns for energy scaling in tapered amplifiers. The Raman effect can be accurately included in our model as a delayed third-order nonlinear response, however, sufficient increase in temporal grid resolution is needed to capture frequencies lying at least 13 THz lower than the pulse frequency, where Raman gain is maximized.

Next, the effect of refractive index changes of active ions due to population dynamics requires detailed study. It is known that this effect along with temperature variations of refractive index may lead to modal instability in high average power amplifiers [16]. Our numerical experiments demonstrate that this instability does not develop on nanosecond time scales, which is also supported by previous studies giving characteristic instability time of the order of upper state lifetime.

Nevertheless, direct modeling of amplification of several consecutive pulses in a train, in which individual pulses respond to the inversion distribution modified by the previous pulses and recovered by the pump, may shed more light on the modal instability development scenario in pulsed amplifiers. We believe that such modeling is possible within reasonable time by further speeding up our numerical code.

7. Conclusion

In conclusion, we present a rather flexible 3D numerical model of an LMA fiber amplifier that enables modeling broadband nanosecond pulses with hundred femtosecond resolution, fully taking into account transverse variations of refractive index profile and distribution of active ions, wavelength dependence of emission and absorption cross sections, gain saturation and Kerr nonlinearity. We used our model for tapered Yb-doped fiber amplifiers and showed that single-mode propagation is maintained along the taper, even in the presence of strong Kerr nonlinearity and saturated gain. The influence of fiber taper bending and core irregularities was studied to demonstrate relatively low excitation of HOMs, which are not further amplified by nonlinear interactions. About 3 mJ of output energy can be extracted in 1 ns pulse from the amplifier tapered from 10 to 110 μm with single-mode beam quality. We also investigated numerically the capabilities of compression and coherent combining of up to 36 perturbed amplifying channels and showed 72% combining efficiency even with up to 11% of HOM content in individual channels.

Acknowledgments

We appreciate the support from the Ministry of Education and Science of Russia (Agreements No. 11.G34.31.0011 and No. 02.B.49.21.0003).

#222879 - $15.00 USD Received 16 Sep 2014; revised 19 Oct 2014; accepted 28 Oct 2014; published 6 Nov 2014